Photoacoustics 32 (2023) 100530

Contents lists available at ScienceDirect

Photoacoustics

journal homepage: www.elsevier.com/locate/pacs

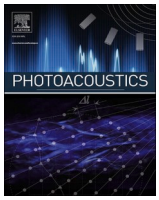

Non-invasive evaluation of transdermal drug delivery using 3-D transient triplet differential (TTD) photoacoustic imaging

Yang Xie [a,1], Huayi Wu [a,1], Ziyan Chen [a], Qi Sun [a], Xiangdong Liu [a], Jinsheng Jiang [b], Bo Wang [b,*], Zeyu Chen [a,*]

[a] School of Mechanical and Electrical Engineering, Central South University, Changsha 410083, China
[b] Department of Biomedical Engineering, School of Basic Medical Science, Central South University, Changsha 410083, China

ARTICLE INFO

Keywords:
Evaluation of transdermal drug delivery
Transient triplet differential (TTD) method
Photoacoustic imaging
3D imaging
Non-invasive
Background-free

ABSTRACT

Transdermal drug delivery (TDD) is less invasive and avoids first-pass metabolism, making it an attractive method for treating various diseases such as diabetes and hypertension. However, current methods for evaluating TDD systems lack in vivo descriptions of drug distribution in the skin. In this study, we demonstrate the capability of the Transient Triplet Differential (TTD) method, a non-invasive and background-free photoacoustic imaging technique, for accurately mapping drug distribution and evaluating different TDD systems. Our findings show that the TTD method can provide high sensitivity and specificity for targeted drug extraction and visualize 3D drug distribution in the skin. Furthermore, in vivo experiments confirmed the potential of the TTD method in evaluating the clinical performance of TDD. It's predictable that the TTD method can be a reliable and non-invasive approach for evaluating TDD systems and offer valuable insights into TDD research and development.

1. Introduction

Transdermal drug delivery (TDD) has received much attention in recent years due to its unique advantages over oral administration and intravenous injection. Specifically, TDD enables sustained and controlled drug release without the first-pass effects and offers a minimally invasive and patient-friendly administration method [1–4]. TDD has found widespread application in the treatment of skin disorders, such as eczema [5], cutaneous infections [6], and skin cancers [7], and holds promise for further development with the emergence of new TDD systems such as sonophoresis, electroporation and microneedles [8,9]. However, current methods for evaluating the performance of TDD systems, such as in vitro penetration experiments and optical imaging, have some limitations. These methods provide limited information about drug distribution and may not be optimal for evaluating the effects of various TTD systems [10].

Typically, the efficiency of TDD systems is evaluated using the Franz diffusion cell, which measures the diffusion of drugs across the skin to a receptor fluid reservoir [11,12]. However, it can only quantitatively describe drug permeation rate and the drug distribution in skin can't be represented. The frozen sections of skin model are often supplemented to further show the effects of TDD systems. However, the skin sections can only provide a two-dimensional view of drug distribution ex vivo, making it impossible to observe drug distribution in vivo [13–16].

Optical imaging techniques, including Confocal Raman spectroscopy (CRS) have also been widely used to describe the distribution of topical drug and evaluate TDD systems. CRS allows for the acquisition of information about the molecular structure of tissue components without using fluorescent labels or chemical stains, and can provide a 3D visualization of topical drug distribution with high spatial resolution in vitro and in vivo [17–20]. However, rapid attenuation of light in tissue limits its imaging depth with only probing several tens of micrometers of skin, while the thickness of human skin typically ranges from 0.5 mm to 4 mm.

Photoacoustic imaging (PAI) may be an ideal solution. As a molecular and non-invasive imaging technique, PAI shows a huge potential in evaluating the effect of transdermal drug delivery systems, which can map the distribution of targeted chromophore with high resolution and great penetration depth by collecting the photoacoustic signals generated by specific pulse laser [21–25]. However, the background signal from endogenous agent such as hemoglobin in the skin disturbs the imaging of the targeted chromophore, which reducing the reliability of the acquired image [26,27].

* Corresponding authors.
E-mail addresses: bowang0302@csu.edu.cn (B. Wang), zeyuchen@csu.edu.cn (Z. Chen).
[1] Co-first authors

https://doi.org/10.1016/j.pacs.2023.100530
Received 21 April 2023; Received in revised form 31 May 2023; Accepted 8 July 2023
Available online 15 July 2023

To overcome this limitation, transient triplet differential (TTD) photoacoustic imaging has been developed as an attractive method that can suppress strong background signal [28,29]. TTD method can extract the transient photoacoustic signals from the triplet state absorption, which is a special characteristic of phosphorescence capable dyes and not normally present among intrinsic chromophores of biological tissue. This means TTD images is of high specificity and free of background signal intervention. However, the board application of TTD imaging is hindered by its long scanning time. In previous study we reported a novel automatic interleaved data acquisition method for TTD imaging and obtained 3D background-free TTD images [30]. The 3D TTD method can be a promising tool to evaluate the TDD systems by accurately acquiring the 3D distribution maps of model drug within the skin.

In this study, we used 3D TTD photoacoustic imaging system to evaluate different transdermal delivery methods by visualizing the 3D distribution of model drug in skin. This innovative approach can obtain accurate drug penetration information in vivo and contribute to the development of advanced TDD systems.

2. Material and methods

2.1. Material

The model drug we used in this work is methylene blue (MB), a phosphorescent dyes commonly used in transient triplet differential (TTD) method. MB is known to have a high phosphorescent quantum yield for triplet state transition and a long triplet lifetime, which enables the transient photoacoustic can be easily detected [30]. The lifetime of MB is influenced by the oxygen content and concentration [31]. In a standard aqueous solution with a concentration of 800 μmol/L, the lifetime of MB is approximately 1 microsecond (Fig. S1). MB shows a peak absorption at 665 nm, and the MB in the triplet state can be fully excited by the laser at about 840 nm (Fig. S2) [32]. At these wavelengths, tissue optical absorption is relatively low, allowing imaging at a larger penetration compared to other materials. As shown in Fig. S3, the photoacoustic signal of MB is basically consistent within 15 min of irradiation with OPO pulsed laser, demonstrating its good photostability. Furthermore, MB is a commonly used FDA-approved water-soluble dye, enabling us to easily observe its distribution within the sample.

2.2. The principle of the TTD method

Fig. 1(b) illustrates the principle of the TTD photoacoustic imaging method. The pump laser is applied to pump the MB from ground singlet state to excited singlet state (S1 to S2). After intersystem crossing (ISC), MB transmits from excited singlet state to triplet state (S2 to T1). T1 will be excited by the probe laser to the other triplet state (T1 to T2). Then, MB generates a photoacoustic signal during the relaxation to T1 (T2 to T1). Notably, transient photoacoustic signals can be generated only when the pump and probe lasers are combined, and the background photoacoustic signals can be obtained when the pump or probe laser works alone. Thus, the TTD photoacoustic signal from the MB in triplet state (T1) can be calculated as:

$$S_{TTD} = S_{pump+probe} - S_{pump} - S_{probe}$$

Here, $S_{pump+probe}$ is the photoacoustic signal obtained by co-excitation of pump and probe laser. S_{pump}(S_{probe}) is the background signal of pump (probe) laser. By such a transient triple differential method, the transient photoacoustic signal of the MB in the T1 state can be separated, which makes the TTD image highly specific and free from interference of other chromophores.

2.3. TTD system set-up

As seen as Fig. 2(b), TTD photoacoustic imaging system is primarily composed of two tunable OPO lasers, a digital delay/pulse generator (DG645, Stanford Research Systems, CA), a three-axis stepper stage, a 7.8 MHz ultrasound linear transducer (L11–5v), and a 256/256 channel Verasonics ultrasound imaging system. One OPO laser (SpitLight OPO 600 broad-band, pumped with 355 nm, 20 Hz) is operated at 665 nm for MB excitation, and the other OPO laser (SpitLight OPO 600 mid-band, Innolas, München, Germany, pumped with 532 nm, 20 Hz) was tuned to 840 nm. The pump and probe lasers were coupled into a 1 × 2 fiber bundle with a beam combiner. The output end of the 1 × 2 fiber bundle with a rectangular output shape, measuring 12 mm in length and 1 mm in width was fixed at the two sides of the ultrasound linear transducer. The resulted fluence on the sample was 5 mJ/cm^2 for the pump laser and 8 mJ/cm^2 for the probe laser.

2.4. Synchronization control and data acquisition

Fig. 2(a) is the sequence diagram of the proposed system. As mentioned above, to get the TTD image, there are three sequences which need to be collected respectively: $S_{pump+probe}$, S_{pump} and S_{probe}. Two OPO lasers should excite MB together to acquire the $S_{pump+probe}$ and work independently when collecting the $S_{pump}$and S_{probe}. Instead of manually switching the state of the OPO lasers, we adjusted the fire time of two lasers periodically relative to data acquisition (DAQ) to get the three sequences as soon as possible. Here, Verasonics system sends out a 20 Hz pulse to synchronize the DDPG which controls OPO's output by two pulses (Flash and Q-swtich), and the OPO emits laser upon the rising edge trigger of the Q-switch (QS) pulse. Specifically, when the DDPG is triggered by the first pulse, it makes the two lasers fire simultaneously at

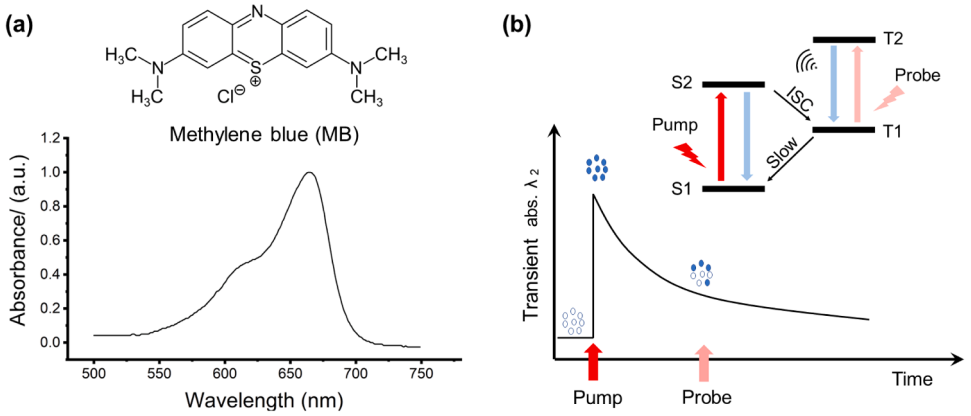

Fig. 1. The principle of TTD method. (a), Molecular formula and absorption spectrum of methylene blue (MB). (b), The principle of TTD method. MB is excited by pump laser to a excited singlet state (S2). After intersystem crossing (ISC). MB in triplet state (T1) is generated. Then probe laser is applied to excite the T1 state to T2 state for generating transient photoacoustic signals.

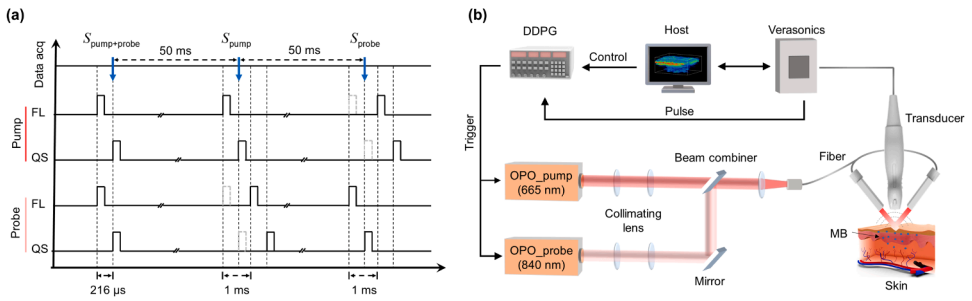

Fig. 2. The TTD photoacoustic imaging system. (a), The synchronization control of the data acquisition method. OPO lasers are triggered by two pulses, flash (FL) and Q-switch (QS), with an interval of 216 μs to ensure stable triggering. 1 ms delay was applied to the probe (pump) laser when we only needed to acquire the S_{pump}(S_{probe}). (b), The schematic of the system. The system mainly includes two OPO lasers, one Verasonics data acquisition system, one DDPG (digital delay/pulse generator), and one transducer array.

the timing of the DAQ to collect the $S_{pump+probe}$. Then, when the DDPG is triggered by the second pulse after 50 ms, it makes the probe laser is fired one millisecond after the DAQ to collect the S_{pump}. Because the time delay of the probe laser is much longer than the data acquisition length (130 μs) and the triplet lifetime (approximately 1 μs), only the background signal of the pump laser will be acquired. Similarly, when the third pulse occurs after 50 ms, only the pump laser is fired one millisecond after the DAQ to collect the S_{probe}. Finally, the whole process will cycle 50 times to average fluctuation of the laser energy. By this means, both OPO lasers are fired continuously at about 20 Hz and the process of the DAQ can be completed at once, which improves the efficiency and stability of data collection.

2.5. 3D imaging method

Ultrasound linear transducer was stabilized on a three-axis stepper stage and motorized horizontally to acquire 3D data. Specifically, the step size was carefully set to 0.2 mm with a scanning distance of 10 mm for imaging porcine skin, and 0.1 mm with a scanning distance of 6 mm for imaging hindlimbs. The acquisition process lasted for a duration of about 8 min, with a total average of 50 scans performed. After data acquisition, 2D images were reconstructed by the backprojection algorithm, then all images were normalized to their maximum values and imported into Amira (version 5.4.0, Thermo Fisher Scientific) for 3D reconstruction.

2.6. Phantom model preparation

In this study, two phantom models were prepared to validate the ability of TTD system to extract the dye and remove the background. In the first phantom model, two PVC tubes (2.2 mm outer diameter and 1.6 mm inner diameter) filled with black ink and MB (800 μmol/L) respectively were buried in a phantom (5 % fat milk and 5 % agar powder). Here, the black ink simulated a strong background signal, and the MB (800 μmol/L) was the target to be extracted. Furtherly, in the second phantom model, there are four PVC tubes filled with bovine hemoglobin and MB of different concentrations in a phantom. Here, the concentrations of MB for the four tubes were 0, 100, 200, and 400 μmol/L and the MB was mixed with the same bovine hemoglobin solution (120 g/L) which simulated the blood except for the 400 μmol/L MB solution.

2.7. Porcine skin model preparation

To prove that the TTD method can accurately map the drug distribution in skin and distinguish the characteristics of different transdermal drug delivery systems, porcine skin models were prepared and imaged. First, fresh porcine skins (approximately 2 cm × 2 cm) were respectively injected with 100 μL MB solution (800 μmol/L) by four different transdermal drug delivery systems (ultrasonic microneedle array (USMA), microneedles, ultrasound import, and free diffusion). Fig. 3 is schematic diagrams of four transdermal drug delivery systems. Here, the microneedles system utilizes a 4 × 4 microneedle array (34-gauge needle model) with an inoculation area measuring 4 × 4 mm. The sonophoresis system primarily involves an ultrasonic transducer module with a central frequency of 118 kHz. The USMA system combines both the microneedle array and the ultrasonic transducer module, which share the same setup as sonophoresis and microneedles methods. In contrast, MB was dropped directly on the skin as a free diffusion system. Then, after continuous administration for 30 min to allow sufficient diffusion of the MB, porcine skins were wrapped in transparent polyethylene film with their surfaces coated with ultrasonic coupling agent. Next, porcine skins were mounted on a horizontal acrylic holder and placed in water tank. After data acquisition with ultrasound linear transducer, porcine skins were sectioned and observed by optical microscope (WST-4KCH, 4KHD) to verify the TTD results.

2.8. In vivo model preparation

The in vivo models were prepared with C57BL mice for about eight weeks. The hindlimbs of mice with hair removed were separately administered with 100 μL MB solution (800 μmol/L) by four transdermal drug delivery systems (ultrasonic microneedle array (USMA), microneedles, sonophoresis, and free diffusion). All transdermal drug delivery systems were the same as those employed for injecting porcine skin. The administration time lasted 15 min, which was just enough to prevent the drug from overflowing due to too fast injection and allow sufficient diffusion of the MB. After administration, the MB remaining on the skin surface was wiped off to only measure corresponding drug distribution in skin. Then, mice were fixed on a 45° tilted acrylic holder and imaged in water bank without the risk of submerging the mice, while being kept anesthetized with a 2 % isoflurane dose and a flow rate of approximately 0.6 L/min. All procedures involving the in vivo animal experiment were approved by the animal ethics committee of Central South University, China.

3. Results

Fig. 4 shows the advantages of the TTD method in removing background and demonstrates its capability for mapping the drug distribution after transdermal drug delivery. In the first phantom experiment, the optical absorption of the MB solution with a concentration of 800 μmol/L is close to the black ink solution, so the tube filled with MB has a similar photoacoustic intensity as tube filled with the black ink, as seen in the conventional PA image of Fig. 4(a). However, the ink signal is dramatically suppressed with the TTD method by extracting the transient signal of the MB in T1 state. Numerical analysis shows that the peak signals ratio of MB to ink improved 7.7 times with the TTD method compared with that in the conventional PA image. In the second phantom experiment, as seen as the Fig. 3(b), the TTD peak signals of the tubes are proportional to the concentrations of the MB in tubes, which means that although the MB is mixed with the bovine hemoglobin solution which has a high concentration of 120 g/L, the TTD method still only extracts the signal of the MB. Compared with conventional PA image in Fig. 3(b), the TTD image exactly describes the distribution of MB in the imaging plane.

In Fig. 4(c), MB in porcine skin was imaged with conventional PA and TTD method. Here, MB was deliveried by ultrasonic microneedle array (USMA), a novel TDD system reported by our group [31]. As

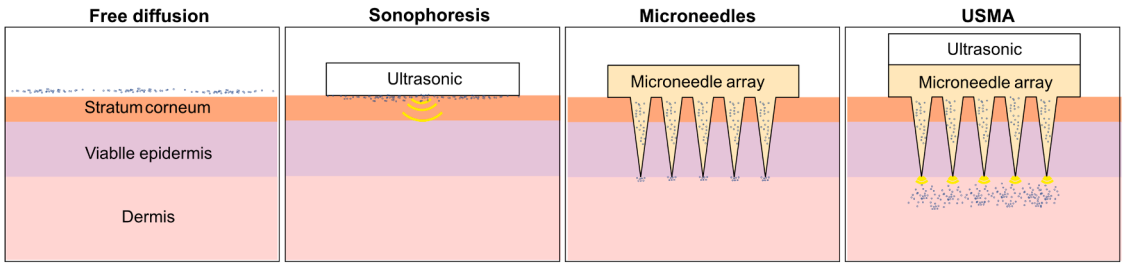

Fig. 3. The schematic diagrams of four transdermal drug delivery systems. Here, ultrasonic microneedle array (USMA) consists of the microneedle array and the ultrasonic transducer module, which share the same setup as sonophoresis and microneedles.

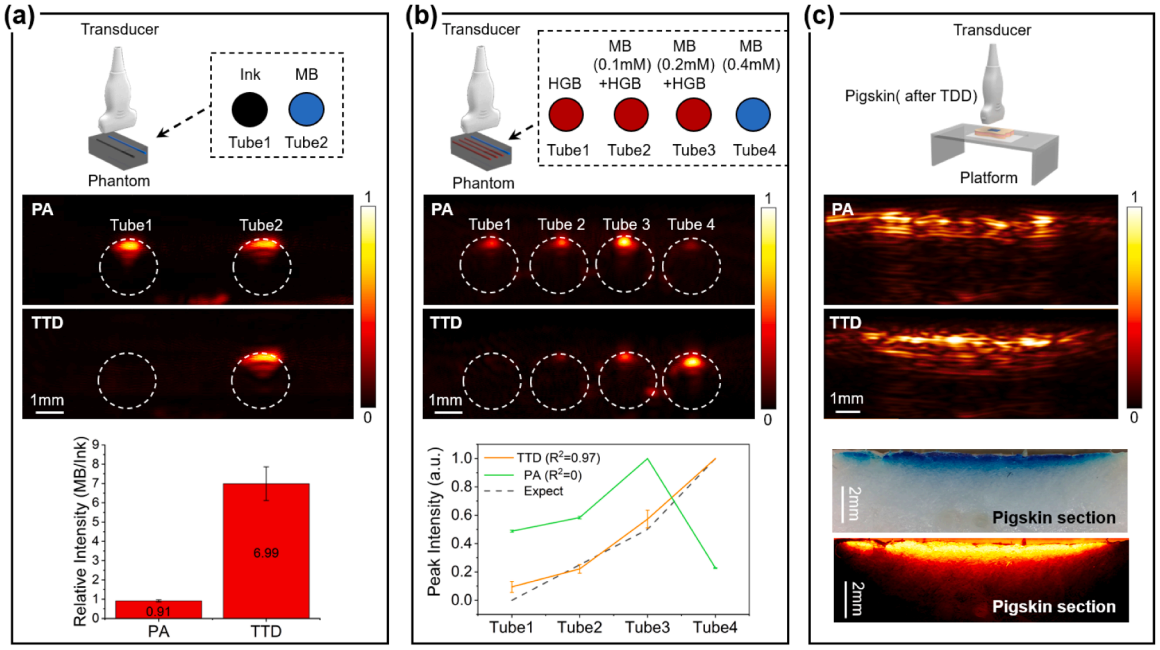

Fig. 4. The advantages of the TTD method in extracting the MB and removing the background. (a), The TTD and conventional PA (665 nm) results of the first phantom experiment. Here, the peak signal ratio between methylene blue and ink is significantly improved from 0.91 in conventional PA image to 6.99 in TTD image. (b), The TTD and conventional PA (665 nm) results of the second phantom experiment. A strong correlation (R^2 = 0.97) was observed between the peak signal intensity ratio among the four tubes and the concentration of MB within the tubes, while effectively suppressing the background signal from hemoglobin (HGB). (c), 2D distribution maps of MB in porcine skin with conventional PA (665 nm) and TTD method. The porcine skin section image is used to test the results, and blue color channel was isolated from the original section image to highlight MB. (For interpretation of the references to color in this figure legend, the reader is referred to the web version of this article.)

shown in the section of porcine skin, it can be seen that the MB at the core area where the MB was injected would be delivered to the depth. Compared with the conventional PA image, the TTD image is closer to the section. Background signals from the porcine skin (such as protein, lipid and melanin) disturb the mapping of the MB in PA image, seeing that almost all the strong signals are in a thin layer at the surface. Notably, the difference between both methods when imaging the porcine skin is not remarkable as before, due to lack of strong background like blood.

Fig. 5 demonstrates the ability to obtain 3D TTD images and evaluate performance of various transdermal drug delivery system. As seen as Fig. 5(a)-(d), different 3D distribution of MB in porcine skin is displayed, corresponding to four transdermal drug delivery system: ultrasonic microneedle array (USMA), microneedles, sonophoresis, and free diffusion. In the free diffusion group, MB mainly distributed on the surface of the skin. In the sonophoresis group, more MB entered the superficial skin layer, but there was almost no distribution of MB in the deep skin layer. In the microneedles group, the penetration depth of MB was deeper. In the USMA group, under the combined effect of the ultrasound field and microneedle penetration, much MB was delivered to the deeper layers of the porcine skin. This result is consistent with the effects of the three TDD methods in animal and clinical studies [33], and verified by porcine skin sections in Fig. 5(e)-(h).

To further verify 3D TTD imaging, we carefully examined the spatial distribution of MB throughout the entire space. Fig. 5(i) presents an isometric 2D slice of the 3D TTD image in the XZ plane, showing the distribution of MB in different cross-sections throughout the administration area. Fig. 5(j) shows the actual distribution of MB in different cross-sections of porcine skin. Compared Fig. 5(i) and Fig. 5(j), we can see that the spatial distribution of MB exhibited by 3D TDD imaging is highly consistent with the actual distribution of MB in porcine skin. Here, most of the MB distributed in central area of administration, and the penetration depth of MB noticeably decreases from the center of the administration area towards the two sides.

To validate the effectiveness of TTD in evaluating the efficacy of TDD in vivo, we conducted tests using mice. Fig. 6(a) shows the hindlimbs of mice which administrated with MB using different TDD systems: ultrasonic microneedle array (USMA), microneedles, sonophoresis, and free diffusion. Fig. 6(c), (g), (k) and (o) are the 3D ultrasound images showing the scan area, while Fig. 6(d), (h), (l) and (p) are the corresponding TTD results. Additionally, the peak intensity of TTD results in Fig. 6(b) were compared. A comparison of these results reveals distinct differences in the penetration and distribution of MB among the different TDD systems. Specifically, the USMA and microneedles group

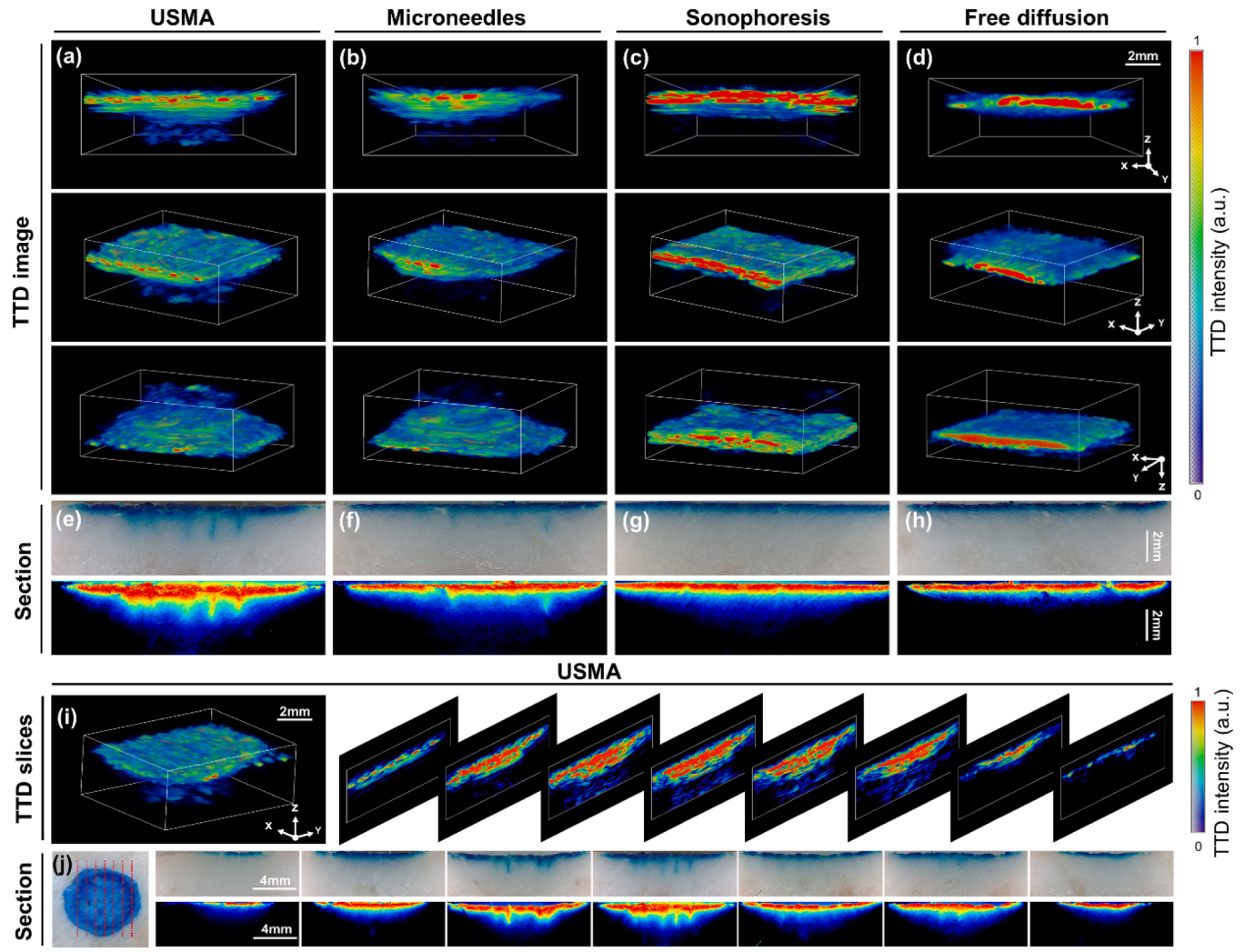

Fig. 5. 3D distribution maps of MB corresponding to different transdermal drug delivery methods, imaged using the TTD system. (a)-(d),The 3D distribution of MB in porcine skin at three views after injection using ultrasonic microneedle array (USMA), microneedles, sonophoresis, and free diffusion. (e)-(h), Porcine skin sections at the central region corresponding to (a)-(d). (i), TTD slices obtained from eight equally spaced XZ plane sections of (a). (j), The porcine skin sections through the whole injected area corresponding to (i), and red dashed lines correspond to the images from left to right. (For interpretation of the references to color in this figure legend, the reader is referred to the web version of this article.)

exhibit more pronounced and stronger MB signals, indicating a deeper penetration facilitated by the microneedle array. Notably, the combined effect of ultrasound and microneedle penetration in the USMA group demonstrates the most effective drug delivery, as evident in Fig. 6(b). In contrast, the sonophoresis and free diffusion groups show relatively low penetration, with MB primarily localized in the superficial layer of the skin. Besides, Fig. 6(f), (j), (n), and (r) intuitively show the distribution of MB at different depths corresponding to the four TDD systems, with the USMA having the deepest penetration, followed by the microneedles, and then the sonophoresis and free diffusion. Importantly, the results obtained from in vivo experiments align well with those obtained from the porcine model, enhancing the reliability of the different TDD systems' performance evaluation.

4. Discussion

Evaluating delivery efficiency and monitoring penetration effect are critical for developing advanced transdermal drug delivery (TDD) systems. In this study, we have demonstrated the capability of the TTD method, a background-free photoacoustic imaging technique, to accurately map the drug distribution in skin and evaluate different TDD systems.

The results of phantom experiments show that TTD method is highly sensitive to the targeted model drug without interference from endogenous contrast agents such as melanin and hemoglobin, which is a significant improvement over conventional photoacoustic imaging techniques and ensures reliability of the TTD methods in evaluating the effect of transdermal drug delivery systems. In addition, our in vitro experiments with porcine skin demonstrated the accurate presentation of the 3D distribution maps of drug and the ability to intuitively distinguish the characteristics of different TDD systems. Besides, we have proved that the TTD method can evaluate effectiveness of TDD systems in vivo.

Although there are many mature methods that can be used to evaluate TTD systems such as Franz diffusion cell, frozen sections of skin models and confocal Raman spectroscopy technique, TTD methods still offers distinct advantages. Firstly, the TTD method can non-invasively extract the target with high specificity, which makes it more applicable in vivo experiments. Secondly, attributed to the superior deep penetration capability of photoacoustic imaging, the TTD method allows for the identification and imaging the target within the entire skin, whose thickness typically ranges from 0.5 mm to 4 mm. In contrast, the Confocal Raman spectroscopy has a limited imaging depth, as it can only probe the top few micrometers of the skin. Finally, the TTD method can

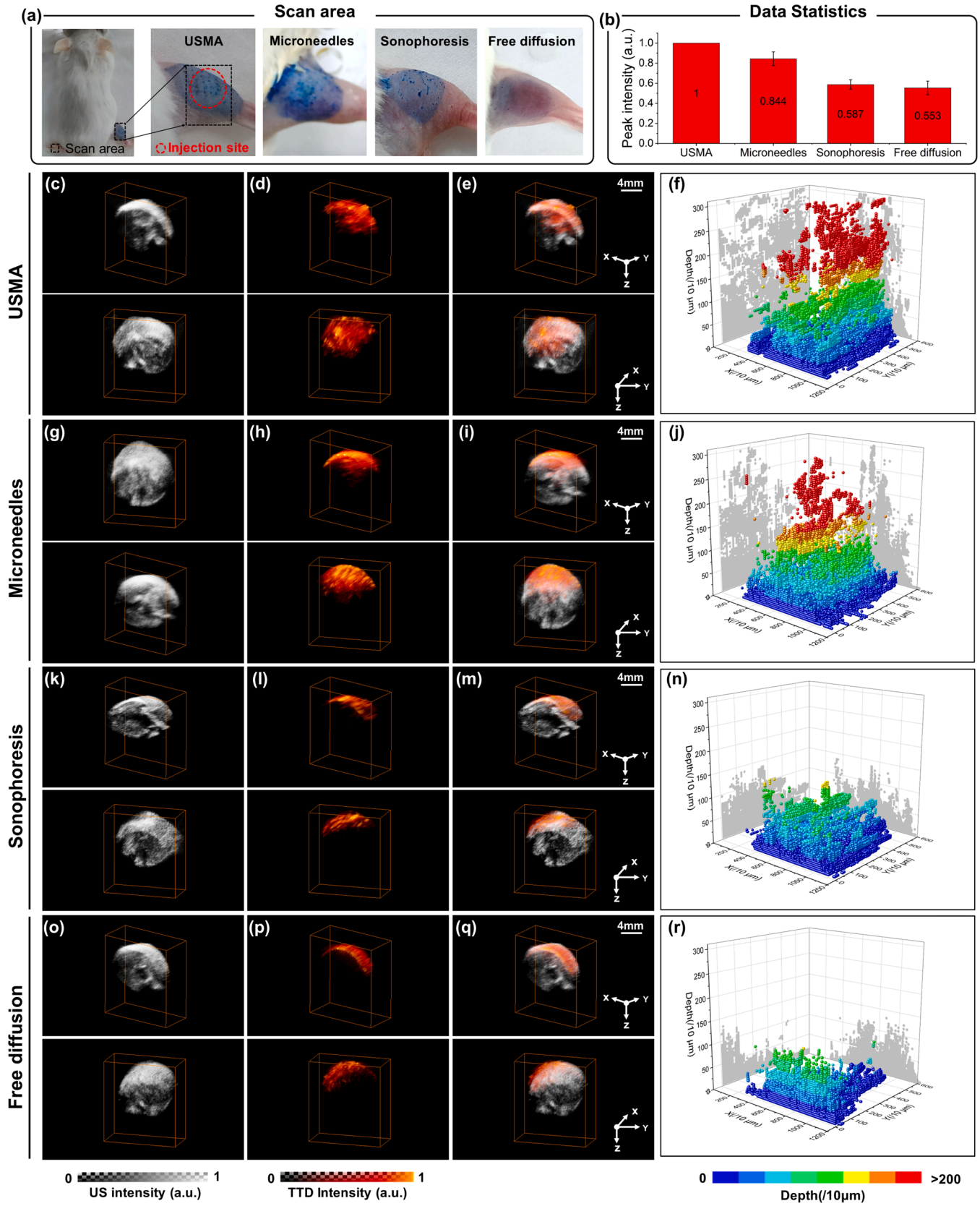

Fig. 6. 3D distribution maps of MB in vivo corresponding to four different TDD methods. (a), Photos of the mice's hindlimb after injection with four TDD systems: ultrasonic microneedle array (USMA), microneedles, sonophoresis, and free diffusion. (b), The peak intensity of four TTD results. (c), 3D ultrasound images of hindlimb for USMA group. (d), 3D TTD images of hindlimb for USMA group. (e), Overlayed images of (d) onto the ultrasound image (c). (g)-(i), 3D images of hindlimb for microneedles group. (k)-(m), 3D images of hindlimb for sonophoresis group. (o)-(q), 3D images of hindlimb for free diffusion group. (f), (j), (n), and (r) distribution of pixel points of TTD images in the depth direction. Here, the maximum pixel values for each column of TTD intensity were selected and aligned in the same row. Then, effective pixel coordinates were extracted using a threshold of 0.1 times the peak intensity and plotted in a 3D scatter plot.

conveniently provide 3D drug distribution maps, which directly reflects the characteristics and effects of TDD systems. This is in contrast to the cumbersome process of frozen sections, which requires sectioning the tissue and staining it before imaging. It is mentioned that Confocal Raman spectroscopy also can present a 3D drug distribution, but it is limited by the imaging speed due to point-by-point scanning mode.

However, the TTD method dose have some limitations that should be acknowledged. Firstly, exogenous contrast agents used in TTD must be phosphorescence-capable dyes, therefore, TTD cannot be used to evaluate the penetration effect of different drugs. Additionally, the TTD method requires an expensive laser system and complex synchronization, which limits the board application of it. Meanwhile, the TTD result in this study had limited spatial resolution due to the low center frequency of the transducer and large step size of the three-axis stepper motors. To address this limitation, future studies could use a higher center frequency transducer, particularly when only drug distribution within a depth of a few millimeters is of interest.

Overall, the TTD method has shown promise in evaluating transdermal drug delivery systems by providing reliable, non-invasive, and 3D imaging of drug distribution. With continued development, it has the potential to become a valuable tool in the development and evaluation of advanced transdermal drug delivery systems.

5. Conclusions

In conclusion, the TTD method is a promising technique for evaluating transdermal drug delivery systems. Its ability to provide reliable, non-invasive, and 3D imaging of drug distribution makes it a valuable tool for transdermal drug delivery research and development. Despite its limitations, the TTD method shows distinct advantages over traditional methods, such as the ability to get 3D distribution maps throughout the entire skin and non-invasive extraction of targeted drugs with high specificity, make it more applicable in vivo experiments. Furthermore, future studies may benefit from the use of higher center frequency transducers to achieve higher spatial resolution. Overall, We believe that the TTD method has the potential to become an important tool in the field of transdermal drug delivery research and development.

Declaration of Competing Interest

The authors declare that they have no known competing financial interests or personal relationships that could have appeared to influence the work reported in this paper.

Data availability

Data will be made available on request.

Acknowledgements

Funding was provided by the Department of Science and Technology of Hunan Province, High-tech Industry Science and Technology Innovation Leading Program (2020SK2003), Science Fund for Distinguished Young Scholars of Hunan Province (2021JJ10069).

Appendix A. Supporting information

Supplementary data associated with this article can be found in the online version at doi:10.1016/j.pacs.2023.100530.

References

[1] D. Ramadon, M.T.C. McCrudden, A.J. Courtenay, R.F. Donnelly, Enhancement strategies for transdermal drug delivery systems: current trends and applications, Drug Deliv. Transl. Res. 12 (4) (2022) 758–791, https://doi.org/10.1007/s13346-021-00909-6.

[2] V. Rastogi, P. Yadav, Transdermal drug delivery system: an overview, Asian J. Pharm. 6 (3) (2012) 161, https://doi.org/10.4103/0973-8398.104828.

[3] S.A.T. Opatha, V. Titapiwatanakun, R. Chutoprapat, Transfersomes: a promising nanoencapsulation technique for transdermal drug delivery, Pharmaceutics 12 (9) (2020) 855, https://doi.org/10.3390/pharmaceutics12090855.

[4] H. Lee, C. Song, S. Baik, D. Kim, T. Hyeon, D. Kim, Device-assisted transdermal drug delivery, Adv. Drug Deliv. Rev. 127 (2018) 35–45, https://doi.org/10.1016/j.addr.2017.08.009.

[5] P. Carter, B. Narasimhan, Q. Wang, Biocompatible nanoparticles and vesicular systems in transdermal drug delivery for various skin diseases, Int. J. Pharm. 555 (2019) 49–62, https://doi.org/10.1016/j.ijpharm.2018.11.032.

[6] M. Sala, R. Diab, A. Elaissari, H. Fessi, Lipid nanocarriers as skin drug delivery systems: properties, mechanisms of skin interactions and medical applications, Int. J. Pharm. 535 (1–2) (2018) 1–17, https://doi.org/10.1016/j.ijpharm.2017.10.046.

[7] T. Waghule, G. Singhvi, S.K. Dubey, M.M. Pandey, G. Gupta, M. Singh, K. Dua, Microneedles: a smart approach and increasing potential for transdermal drug delivery system, Biomed. Pharmacother. 109 (2019) 1249–1258, https://doi.org/10.1016/j.biopha.2018.10.078.

[8] V. Singh, P. Kesharwani, Recent advances in microneedles-based drug delivery device in the diagnosis and treatment of cancer, J. Control. Release 338 (2021) 394–409, https://doi.org/10.1016/j.jconrel.2021.08.054.

[9] M. Yang, Y.W. Gu, T. Wang, J. Liu, Advancement of lipid-based nanocarriers and combination application with physical penetration technique, Curr. Drug Deliv. 16 (4) (2019) 312–324, https://doi.org/10.2174/1567201816666190118125427.

[10] S. Chaturvedi, A. Garg, An insight of techniques for the assessment of permeation flux across the skin for optimization of topical and transdermal drug delivery systems, J. Drug Deliv. Sci. Technol. 62 (2021), 102355, https://doi.org/10.1016/j.jddst.2021.102355.

[11] J. Park, H. Lee, G. Lim, N. Kim, D. Kim, Y. Kim, Enhanced transdermal drug delivery by sonophoresis and simultaneous application of sonophoresis and iontophoresis, AAPS PharmSciTech 20 (3) (2019) 99, https://doi.org/10.1208/s12249-019-1309-z.

[12] L. Coderch, I. Collini, V. Carrer, C. Barba, C. Alonso, Assessment of finite and infinite dose in vitro experiments in transdermal drug delivery, Pharmaceutics 13 (3) (2021) 364, https://doi.org/10.3390/pharmaceutics13030364.

[13] Y.I. Svenskaya, E.A. Genina, B.V. Parakhonskiy, E.V. Lengert, E.E. Talnikova, G. S. Terentyuk, S.R. Utz, D.A. Gorin, V.V. Tuchin, G.B. Sukhorukov, A simple non-invasive approach toward efficient transdermal drug delivery based on biodegradable particulate system, ACS Appl. Mater. Interfaces 11 (19) (2019) 17270–17282, https://doi.org/10.1021/acsami.9b04305.

[14] H. Jung, M.K. Kim, J.Y. Lee, S.W. Choi, J. Kim, Adhesive hydrogel patch with enhanced strength and adhesiveness to skin for transdermal drug delivery, Adv. Funct. Mater. 30 (42) (2020), 2004407, https://doi.org/10.1002/adfm.202004407.

[15] S. Khan, M.U. Minhas, I.A. Tekko, R.F. Donnelly, R.R.S. Thakur, Evaluation of microneedles-assisted in situ depot forming poloxamer gels for sustained transdermal drug delivery, Drug Deliv. Transl. Res. 9 (4) (2019) 764–782, https://doi.org/10.1007/s13346-019-00617-2.

[16] J. Li, Y. Zhou, J. Yang, R. Ye, J. Gao, L. Ren, B. Liu, L. Liang, L. Jiang, Fabrication of gradient porous microneedle array by modified hot embossing for transdermal drug delivery, Mater. Sci. Eng. C 96 (2019) 576–582, https://doi.org/10.1016/j.msec.2018.11.074.

[17] L. Franzen, M. Windbergs, Applications of Raman spectroscopy in skin research — from skin physiology and diagnosis up to risk assessment and dermal drug delivery, Adv. Drug Deliv. Rev. 89 (2015) 91–104, https://doi.org/10.1016/j.addr.2015.04.002.

[18] S. Zsikó, E. Csányi, T. Kovács, M. Budai-Szűcs, A. Gácsi, S. Berkó, Methods to evaluate skin penetration in vitro, Sci. Pharm. 87 (2019) 19–21, https://doi.org/10.3390/scipharm87030019.

[19] Y. Liu, D.J. Lunter, Profiling skin penetration using pegylated emulsifiers as penetration enhancers via confocal raman spectroscopy and fluorescence spectroscopy, Eur. J. Pharm. Biopharm. 166 (2021) 1–9, https://doi.org/10.1016/j.ejpb.2021.04.027.

[20] G.P.S. Smith, C.M. McGoverin, S.J. Fraser, K.C. Gordon, Raman imaging of drug delivery systems, Adv. Drug Deliv. Rev. 89 (2015) 21–41, https://doi.org/10.1016/j.addr.2015.01.005.

[21] R. Chen, S. Huang, T. Lin, H. Ma, W. Shan, F. Duan, L. Nie, Photoacoustic molecular imaging-escorted adipose photodynamic–browning synergy for fighting obesity with virus-like complexes, Nat. Nanotechnol. 16 (4) (2021) 455–465, https://doi.org/10.1038/s41565-020-00844-6.

[22] G. Huang, J. Lv, Y. He, J. Yang, L. Zeng, L. Nie, In vivo quantitative photoacoustic evaluation of the liver and kidney pathology in tyrosinemia, Photoacoustics 28 (2022), 100410, https://doi.org/10.1016/j.pacs.2022.100410.

[23] J. Lv, Y. Xu, L. Xu, L. Nie, Quantitative functional evaluation of liver fibrosis in mice with dynamic contrast-enhanced photoacoustic imaging, Radiology 300 (1) (2021) 89–97, https://doi.org/10.1148/radiol.2021204134.

[24] Y.Y. Zhou, J.B. Chen, M.S. Li, P.X. Lai, L.D. Wang, Single-shot linear dichroism optical-resolution photoacoustic microscopy, Photoacoustics 16 (2019), 100148, https://doi.org/10.1016/j.pacs.2019.100148.

[25] Y.Y. Zhou, J.G. Ni, C.Y. Wen, P.X. Lai, Light on osteoarthritic joint: from bench to bed, Theranostics 12 (2) (2022) 542–557, https://doi.org/10.7150/thno.64340.

[26] J. Huang, K. Pu, Activatable molecular probes for second near-infrared fluorescence, chemiluminescence, and photoacoustic imaging, Angew. Chem. Int. Ed. 59 (2020) 11717–11731, https://doi.org/10.1002/anie.202003483.

[27] J. Yao, A.A. Kaberniuk, L. Li, D.M. Shcherbakova, R. Zhang, L. Wang, G. Li, V. V. Verkhusha, L.V. Wang, Multiscale photoacoustic tomography using reversibly

switchable bacterial phytochrome as a near-infrared photochromic probe, Nat. Methods 13 (2016) 67–73, https://doi.org/10.1038/nmeth.3656.
[28] J.W.Y. Tan, C.H. Lee, R. Kopelman, X. Wang, Transient triplet differential (Ttd) method for background free photoacoustic imaging, Sci. Rep. 8 (2018) 17457, https://doi.org/10.1038/s41598-018-27578-9.
[29] G. Wang, B. Wang, T. Ye, C.C. Wang, L.L. Guo, J.Y. Xiao, Z.Y. Chen, Ultrasonic ring array-based transient triplet differential photoacoustic imaging for strong background removal, Front. Mater. 8 (2021), 699433, https://doi.org/10.3389/fmats.2021.699433.
[30] B. Wang, Y. Xie, X. He, J.S. Jiang, J.Y. Xiao, Z.Y. Chen, Transient triplet differential-based photoacoustic lifetime imaging with an automatic interleaved data acquisition method for improved scanning speed and stability, Opt. Express 30 (2022) 39129–39144, https://doi.org/10.1364/OE.472132.
[31] E. Morgounova, Q. Shao, B.J. Hackel, D.D. Thomas, S. Ashkenazi, Photoacoustic lifetime contrast between methylene blue monomers and self-quenched dimers as a model for dual-labeled activatable probes, J. Biomed. Opt. 18 (2013), 056004, https://doi.org/10.1117/1.JBO.18.5.056004.
[32] J. Chen, T.C. Cesario, P.M. Rentzepis, Effect of Ph on methylene blue transient states and kinetics and bacteria photoinactivation, J. Phys. Chem. A 115 (2011) 2702–2707, https://doi.org/10.1021/jp110215g.
[33] Z.Y. Chen, H.Y. Wu, S. Zhao, X. Chen, T. Wei, H. Peng, Z. Chen, 3D-printed integrated ultrasonic microneedle array for rapid transdermal drug delivery, Mol. Pharm. 19 (9) (2022) 3314–3322, https://doi.org/10.1021/acs.molpharmaceut.2c00466.

Yang Xie received his B.E. degree in mechanical engineering from Central South University in Changsha, China in 2020. Now he is working to pursue his M.S. degree in mechanical engineering in Central South University. His research interests mainly focus on photoacoustic imaging technologies.

Huayi Wu received his B.E. degree in mechanical engineering from Changsha University of Science and Technology in Changsha, China in 2020. Now he is working to pursue his M.S. degree in mechanical engineering in Central South University. His research interests mainly focus on the research and development of transdermal drug delivery technology.

Ziyan Chen received her B.E. degree in control Technology and Instruments from Hefei University of Technology in Xuancheng, China in 2018. She received M.S. degree in instrument science and technology from Huaqiao University in Xiamen, China in 2021. Now she is working to pursue her Ph. D degree in mechanical engineering in Central South University. Her research interests mainly focus on transdermal drug delivery system.

Xiangdong Liu received his B.E. degree in biomedical engineering from Central South University in Changsha, China in 2021. Now he is working to pursue his M.S. degree in mechanical engineering in Central South University. His research interests mainly focus on ultrasound imaging technologies.

Qi Sun received his B.E. degree in biomedical engineering from Central South University in Changsha, China in 2021. Now he is working to pursue his M.S. degree in mechanical engineering in Central South University. His research interests mainly focus on microfluidic chip design and liposome synthesis.

Jinsheng Jiang received his B.E. degree in biomedical engineering from Central South University in Changsha, China in 2020. Now he is working to pursue his M.S. degree in biomedical Engineering in Central South University. His research interests mainly focus on photoacoustic imaging technologies.

Bo Wang obtained his B.S. (2006) and M.S. (2009) degrees in physics from Tsinghua University. He received his Ph.D. degree in Biomedical Engineering from the University of Florida in 2014. He joined the School of Basic Medical Science at Central South University in 2020 as a distinguished professor. His research interests are mainly in photoacoustic imaging, including system design, reconstruction algorithms, and biomedical applications.

Zeyu Chen is a Professor at the School of Mechanical and Electrical Engineering, Central South University. He received his B.E. degree from Central South University in 2012. He obtained his M.S. and Ph. D degrees from the University of Southern California in 2015 and 2017. His research interests include the diagnosis of skin diseases and the development of ultrasonic and optical-based medical diagnostic equipment and therapeutic instruments.